



Increased drought events in southwest China revealed by tree ring oxygen isotopes and potential role of Indian Ocean Dipole



Chenxi Xu ^{a,b,*}, Wenling An ^{a,b}, S.-Y. Simon Wang ^c, Liang Yi ^d, Junyi Ge ^{b,e,h}, Takeshi Nakatsuka ^f, Masaki Sano ^{f,g}, Zhengtang Guo ^{a,b,h}

^a Key Laboratory of Cenozoic Geology and Environment, Institute of Geology and Geophysics, Chinese Academy of Sciences, Beijing 100029, China

^b CAS Center for Excellence in Life and Paleoenvironment, Beijing 100044, China

^c Department of Plants, Soils, and Climate, Utah State University, Logan, UT, USA

^d State Key Laboratory of Marine Geology, Tongji University, Shanghai, China

^e Key Laboratory of Vertebrate Evolution and Human Origins of the Chinese Academy of Sciences, Institute of Vertebrate Paleontology and Paleoanthropology, Chinese Academy of Sciences, Beijing, China

^f Research Institute for Humanity and Nature, Motoyama, Kamigamo, Kita-ku, Kyoto, Japan

^g Faculty of Human Sciences, Waseda University, 2-579-15 Mikajima, Tokorozawa 359-1192, Japan

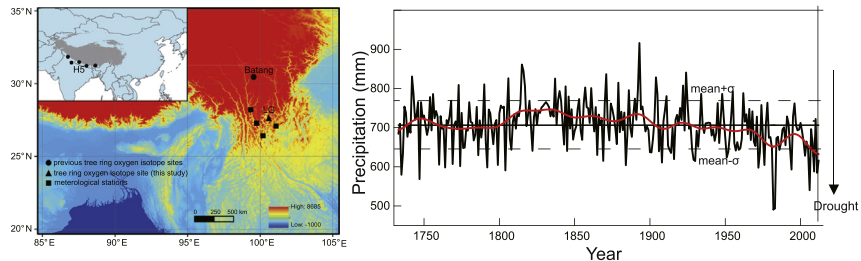
^h University of Chinese Academy of Sciences, Beijing, China

HIGHLIGHTS

- Tree ring oxygen isotopes can be used to reconstruct rainy season precipitation in southwest China.
- The reconstructed precipitation reveals an apparent drying trend since 1840.
- Increased drought events since 1970 likely due to the increase in positive Indian Ocean Dipole events.

GRAPHICAL ABSTRACT

Maps showing the LuGu lake sampling sites (LG, triangle) and from previous study (circle) in Batang and H5 (inset) and meteorological stations (square). The major finding is the right panel showing the reconstructed May–October precipitation from 1733 to 2013, overlaid with an 11-year smooth curves (red lines) emphasize decadal variations. Notice that increased and more intense drought events after 1950.



Maps showing the LuGu lake sampling sites (LG, triangle) and from previous study (circle) in Batang and H5 (inset) and meteorological stations (square). The major finding is the right panel showing the reconstructed May–October precipitation from 1733 to 2013, overlaid with a 11-year smooth curves (red lines) emphasize decadal variations. Notice that increased and more intense drought events after 1950.

ARTICLE INFO

Article history:

Received 23 November 2018

Received in revised form 15 January 2019

Accepted 15 January 2019

Available online 17 January 2019

Editor: Elena Paoletti

Keywords:

Precipitation

Tree ring oxygen isotope

ABSTRACT

The highlands in southwestern China experience pronounced fluctuations in the hydroclimate with profound impacts on agriculture and economics. To investigate the drought history of this region beyond instrumental records, a tree ring cellulose oxygen isotope ($\delta^{18}\text{O}_c$) chronology was developed for the period 1733–2013 using samples collected from six Larix trees in the low-latitude highlands (LLH) of southwestern China. The analysis revealed that $\delta^{18}\text{O}_c$ is significantly correlated with the rainy season (May–October) precipitation and relative humidity, as well as drought severity. The $\delta^{18}\text{O}_c$ chronology accounts for 46% of the observed variance in the rainy season precipitation and it was subsequently used to reconstruct precipitation. The reconstructed precipitation reveals an apparent drying trend since 1840, accompanied by increasingly frequent drought events since 1970. Interdecadal variability is also present, characterized with two distinct wet periods in 1740–1760 and 1800–1900 and two drier periods in 1760–1800 and 1900–2013. On the interannual timescale, the LLH

* Corresponding author at: Key Laboratory of Cenozoic Geology and Environment, Institute of Geology and Geophysics, Chinese Academy of Sciences, Beijing 100029, China.
E-mail address: cxxu@mail.iggcas.ac.cn (C. Xu).

precipitation was modulated collectively by the El Niño–Southern Oscillation (ENSO) and the Indian Ocean dipole (IOD). There appears to be an enhanced precipitation-IOD relationship since 1970 in response to the increase in positive-IOD events, implying an increasing likelihood of drought for the southwest China LLH.

© 2019 Elsevier B.V. All rights reserved.

1. Introduction

Low-latitude highlands (LLH) in China refer to areas where the average altitude exceeds 1500 m above sea level in latitudes south of 30°N. The southwest China LLH are characterized by distinct rainy and dry seasons (Cao et al., 2014). Agriculture and economy in LLH depend on its unique hydroclimate. In 2006, 2009 and 2011, the southwestern China LLH experienced severe droughts during summer and autumn (Peng et al., 2007; Sun and Yang, 2012; Wang et al., 2016; Yang et al., 2012). These severe droughts caused a shortage of drinking water for 21 million people and an economic loss reaching 30-billion USD.

Considerable progress has been made in the understanding of the LLH precipitation's interannual and interdecadal variations (Cao et al., 2014; Liu et al., 2018, 2011). Previous studies found that the El Niño–Southern Oscillation (ENSO) and the Indian Ocean dipole (IOD) can modulate rainy-season precipitation in southwest China LLH (Cao et al., 2014; Liu et al., 2011). However, meteorological records in southwest China that only span 50 years are insufficient to reveal the decadal climate variability associated with ENSO, IOD and precipitation in LLH. Longer-term and higher-resolution records are needed to improve the understanding of the rainy season variability in LLH.

At present, a few high-resolution paleoclimate records with sufficient resolutions existed in southwest China LLH, particularly the moisture-sensitive proxies. The few data sets that do exist include sediment records from Lake Erhai and Lake Lugu, which revealed a centennial change in the Indian summer monsoon precipitation (Sheng et al., 2015; H. Xu et al., 2015), and tree-ring chronologies in adjacent areas depicting the warm-season Palmer Drought Severity Index (PDSI) and cold-season precipitation for several hundred years (Fan et al., 2010; Fang et al., 2010; Gou et al., 2013; Li et al., 2017). Since tree growth is

affected mainly by climate conditions prior to the current or early growing season (Wang et al., 2012; Li et al., 2017), it is difficult to reconstruct the rainy season (May–October) precipitation using tree ring width. Other studies have used historical documents in the Yunnan provincial capital Kunming to infer the year-to-year rainy season variation (Yang et al., 2007). Moreover, records in high-elevation area (>3000 m) were scarce and so, long-term proxy with a strong signal of the LLH's rainy season are also lacking.

Different from tree ring width, tree ring cellulose oxygen isotopes ($\delta^{18}\text{O}_c$) record the precipitation $\delta^{18}\text{O}$ and relative humidity signal during the tree growing season (Roden et al., 2000), while the period of tree growth in monsoon Asia coincides with its distinct rainy season. In the rainy season of monsoon Asia, precipitation $\delta^{18}\text{O}$ and relative humidity are highly correlated (Araguas-Araguas et al., 1998). Previous studies have shown that $\delta^{18}\text{O}_c$ also significantly correlates with the Standardized Precipitation Evapotranspiration Index (SPEI) and relative humidity, so it is feasible to use $\delta^{18}\text{O}_c$ for reconstructing hydroclimate in southern China LLH (An et al., 2013; Liu et al., 2013; Shi et al., 2012; Wernicke et al., 2015; Xu et al., 2012, 2017, 2018b). In this study, a tree ring oxygen isotope chronology was built from six Larch trees collected from southwestern China LLH for two purposes. Firstly, we aim to reconstruct hydroclimate history over the past centuries based on $\delta^{18}\text{O}_c$ chronology. Secondly, we would like to investigate driving factors that affect inter-annual to centennial scale variability of hydroclimate in southwestern China LLH. It is postulated that inter-annual variations of hydroclimate in southwestern China LLH may be mainly influenced by large-scale atmospheric circulation (such as ENSO and IOD), and such teleconnection could be linked to climate modes. Moreover, the long-term hydroclimate in southwestern China LLH may be affected by Indian summer monsoon.

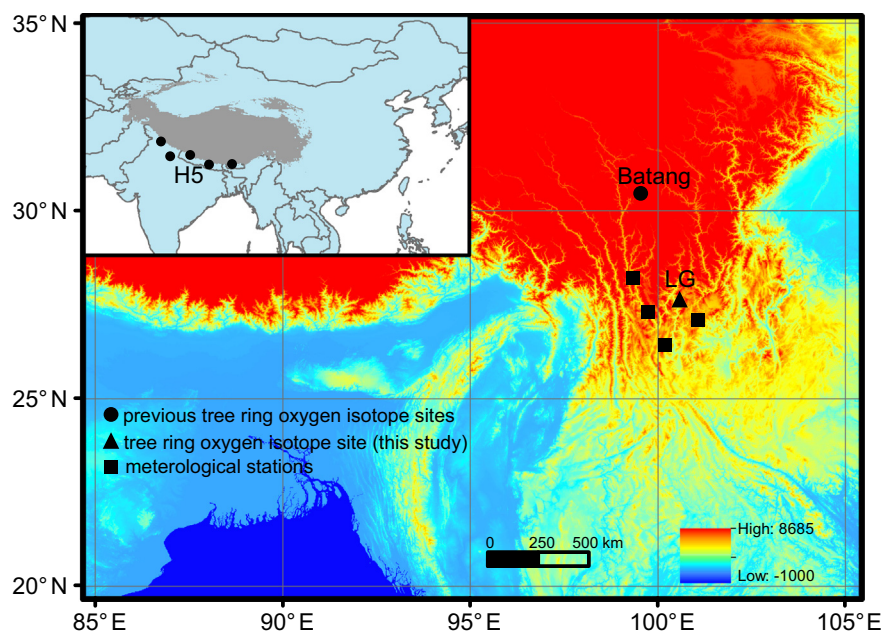


Fig. 1. Map showing the location of LuGu lake sampling sites in this study (LG, triangle) and from previous study (circle) in Batang (An et al., 2013) and southern Himalaya (H5, Xu et al., 2018a), and meteorological stations (square).

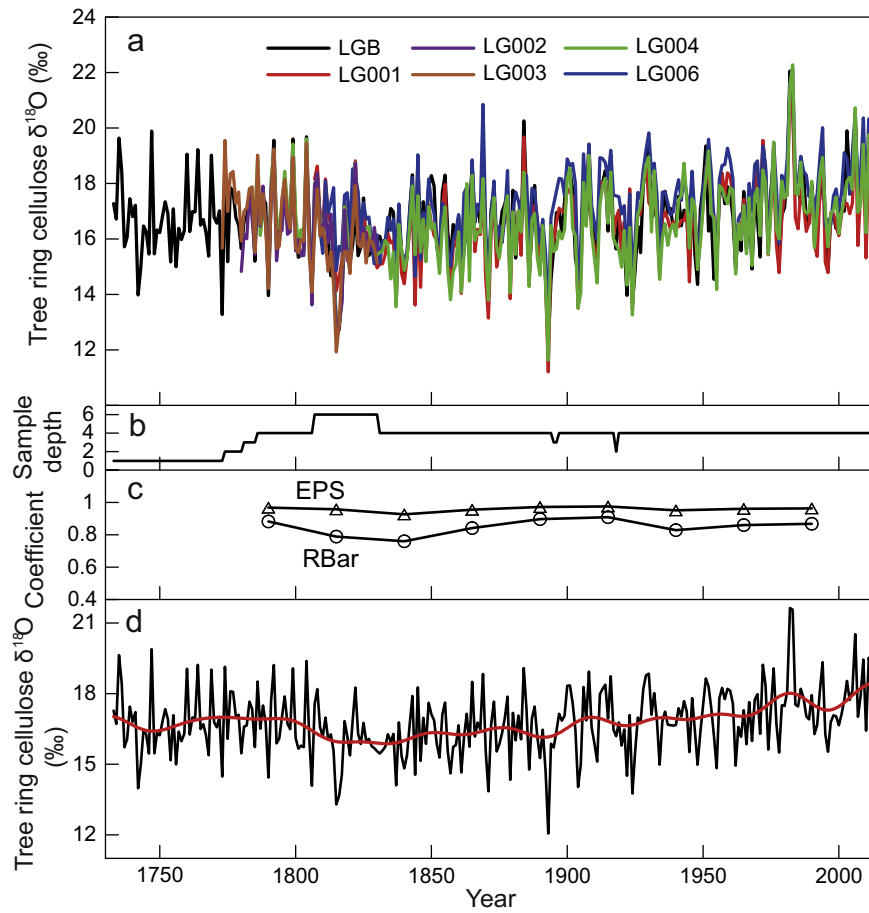


Fig. 2. Tree ring oxygen isotope ($\delta^{18}O_c$) variations from six individual trees (a), sample depth (b), expressed population signal (EPS) and mean inter-trees correlations (Rbar) values (c) and LG $\delta^{18}O_c$ chronology during the period of 1733–2013, 10-year smooth curves (red lines) emphasize decadal variations.

2. Material and methods

2.1. Sampling site and oxygen isotope analysis

Tree ring samples were collected from 23 Larch trees (*Larix potaninii* var. *macrocarpa*) growing in natural forests in Ninglang County, Yunnan

Province, China (27.63°N, 100.64°E, 3300–4000 m a.s.l.); the tree site location is shown in Fig. 1 (labeled LG, which is the abbreviation of LuGu lake area). The local soils is primarily subalpine meadow soils with a thick humus layer (up to 20–35 cm in depth) and well water conditions for plants. The single standing trees are often >10 m from each another. Two core samples from opposite sides of each tree were collected using

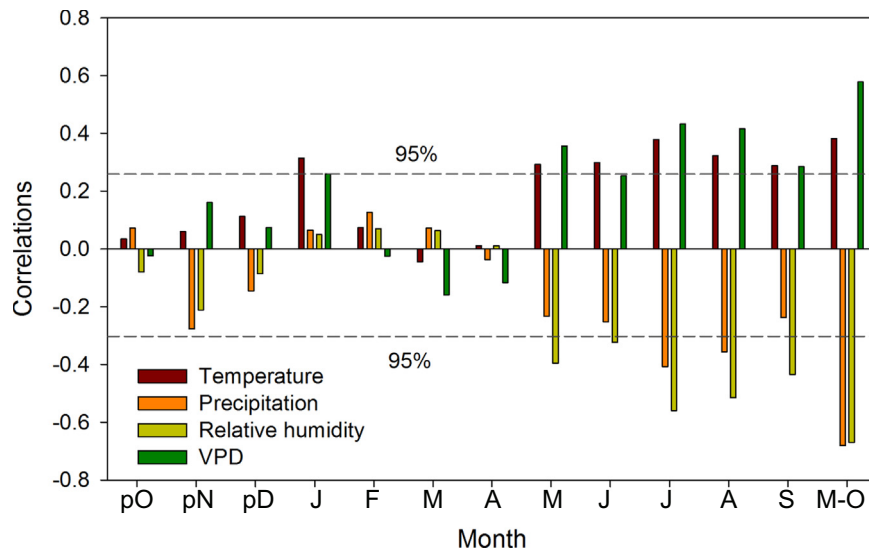


Fig. 3. Correlations between tree ring oxygen isotope with regional monthly temperature, precipitation, relative humidity and vapor pressure deficit (VPD) during the period of 1959–2013.

Table 1
Calibration and verification statistics for the common period of 1959–2013.

Calibration period	r	R ²	Verification period	RE	CE
Full period (1959–2013)	−0.68	0.46	–	–	–
Early half (1959–1986)	−0.80	0.64	Late half (1988–2013)	0.56	0.52
Late half (1987–2013)	−0.57	0.33	Early half (1960–1987)	0.27	0.21

a 12-mm diameter increment borer at breast height. The cores were air dried at room temperature and the surfaces of the cores were smoothed to make the cell structure clearly visible. The ring widths of all cores were then measured, at a resolution of 0.01 mm using a binocular microscope with a linear stage interfaced with a computer (Velmex™, Acu-Rite). Cross dating was performed by matching the variations in ring width from all trees cores to determine the absolute year of each ring. Quality control was completed using the program COFECHA (Holmes, 1983).

Ring width does not affect tree ring oxygen isotopes (Sano et al., 2013; Xu et al., 2016), so six trees with wider rings (Sample Number: LGB, LG001, LG002, LG003, LG004, LG006) were selected for the isotopic analysis. It has been shown that $\delta^{18}\text{O}_c$ of earlywood and latewood can extract climate information in different months (An et al., 2012). In our case, however, the latewood of these samples were too narrow to obtain enough sample material for isotope analysis, so we used the whole annual rings for the oxygen isotope analysis instead. We employed the modified plate method to extract α -cellulose (Xu et al., 2011, 2013). Oxygen isotope ratio ($^{18}\text{O}/^{16}\text{O}$) of cellulose samples was measured using an isotope ratio mass spectrometer (Delta V Advantage,

Thermo Scientific) interfaced with a pyrolysis-type high-temperature conversion elemental analyzer (TC/EA, Thermo Scientific) housed at the Research Institute for Humanity and Nature, Japan. Cellulose $\delta^{18}\text{O}$ values were calculated by comparison with the Merck cellulose (laboratory working standard), which was inserted every eight tree samples during the measurements. Oxygen isotope results are presented in δ notation as the per mil (‰) deviation from Vienna Standard Mean Ocean Water (VSMOW):

$$\delta^{18}\text{O} = ((R_{\text{sample}}/R_{\text{standard}}) - 1) \times 1000,$$

where R_{sample} and R_{standard} are the $^{18}\text{O}/^{16}\text{O}$ ratios of the sample and standard, respectively. The analytical uncertainties for repeated measurements of Merck cellulose were approximately $\pm 0.21\text{‰}$ ($n = 130$).

2.2. Climate and statistical analyses

At present, there is no weather station in the sampling forest. Therefore, we used the closest Deqin, Zhongdian, Yanyuan and Lijiang stations, which are about 239.8 km, 105.7 km, 97.1 km and 95.5 km away from our sampling site. The cities where above stations locate are small with good natural environment. Meteorological data from four meteorological stations near the tree site (Fig. 1) were averaged to represent the regional climate during their common data period of 1959–2013 (Table S1). The climatological annual precipitation is 757.8 mm with the standard deviation of 87.5 mm, 87.6% of which falls in the rainy season from May to October (Fig. S1), which is associated with high temperature and high relative humidity. Monthly vapor

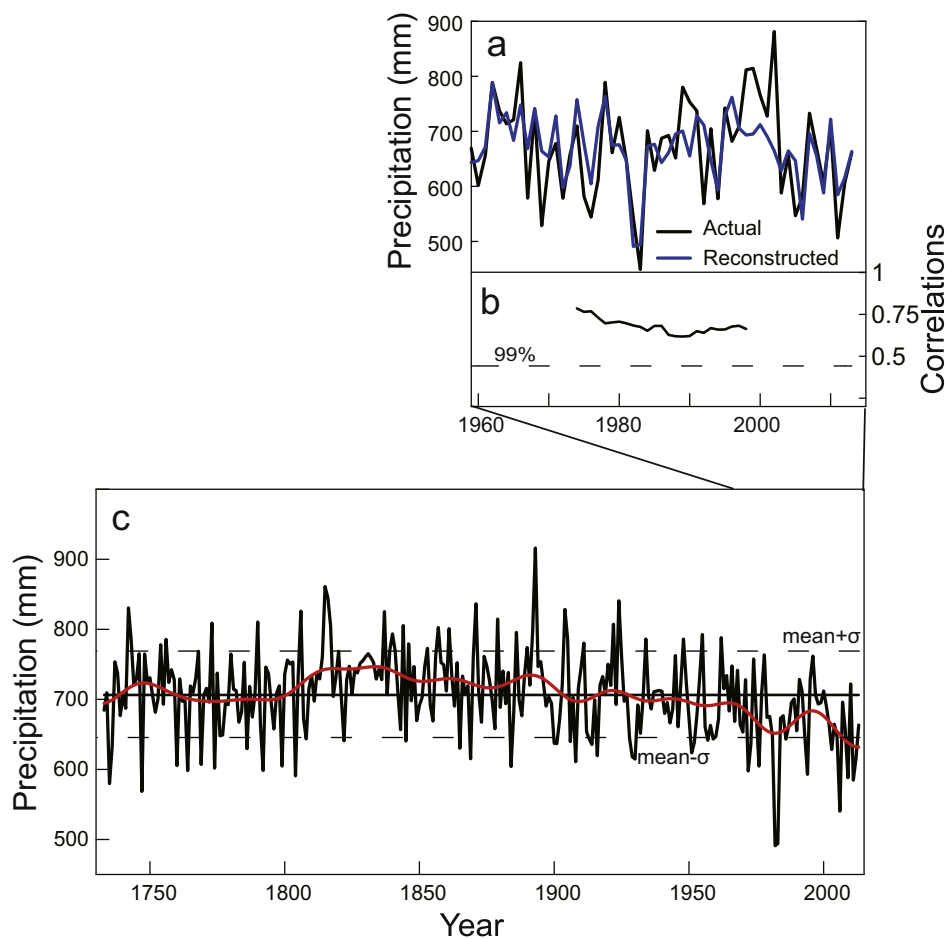


Fig. 4. Reconstructed and actual May–October precipitation (a), 31-year running correlations between them (b), and reconstructed May–October precipitation during the period of 1733–2013, 11-year Fast Fourier Transform (FFT) smooth curves (red lines) emphasize decadal variations.

pressure deficit (VPD) were calculated based on the method of Hogg (1997) and Hogg et al. (2013) to evaluate the relationship between VPD and $\delta^{18}\text{O}_c$.

Besides meteorological stations, we also used gridded, worldwide precipitation data from the CRU TS4.0 and GPCC v7 (Schneider et al., 2015), with a resolution of $0.5^\circ \times 0.5^\circ$, to examine the spatial correlation between $\delta^{18}\text{O}_c$ and regional precipitation. Precipitation time series from CRU and GPCC were interpolated based on precipitation from the meteorological station. The GPCC precipitation product uses considerably more stations than CRU data, CRU TS gridded data was created by interpolating available station observations (Harris et al., 2014). The CRU regional precipitation has excellent agreement with GPCC v5 data. Furthermore, sea surface temperature (SST) data obtained from the National Climatic Data Center v4 (Smith et al., 2008) were used for the investigation of the climate influences on hydroclimate originated from the tropical oceans.

Pearson's correlation was calculated between these four climatic variables and the $\delta^{18}\text{O}_c$ series from previous October to current October during 1959–2013 to investigate climate's influences on $\delta^{18}\text{O}_c$. Correlation analysis was performed on the Royal Netherlands Meteorological Institute Climate Explorer (<http://www.knmi.nl/>). Validity of the linear regression model between $\delta^{18}\text{O}_c$ and hydroclimate was assessed by splitting the samples into two subperiods (1959–1986 and 1987–2013) for separate calibration and verification. Reduction of

error (RE), and coefficient of efficiency (CE) were included in the statistical tests (Cook et al., 1999). The Indian Ocean dipole index DMI was established by Saji et al. (1999), and IOD events changes were derived from and Hochreuther et al. (2016).

3. Results and discussion

3.1. Chronology statistics

Fig. 2 shows the $\delta^{18}\text{O}_c$ time series obtained for six individual trees. Inter-tree $\delta^{18}\text{O}$ variability of the six trees is small ($<1.5\%$), given that inter-tree $\delta^{18}\text{O}$ variability falls within the range of 1–4% (Leavitt, 2010). These $\delta^{18}\text{O}$ data show similar mean values and standard deviations during the common period of 1807–1830 (Table S2), confirming that $\delta^{18}\text{O}_c$ from these six trees reflect common changes, which may indicate these trees grow under a similar hydroclimate. The six $\delta^{18}\text{O}$ series also have significant inter-series correlations (0.76–0.91) at any period in the past 281 years, determined with 50-year running Rbar statistics (Fig. 2c). The accepted expressed population signal (EPS) value is higher than 0.85 (Wigley et al., 1984), and EPS statistic for these six $\delta^{18}\text{O}_c$ time series fell in the range of 0.92–0.97 since the 1790s. These results indicate that the six $\delta^{18}\text{O}_c$ time series share a common variation relatively free of noise, indicating a robust $\delta^{18}\text{O}_c$ chronology.

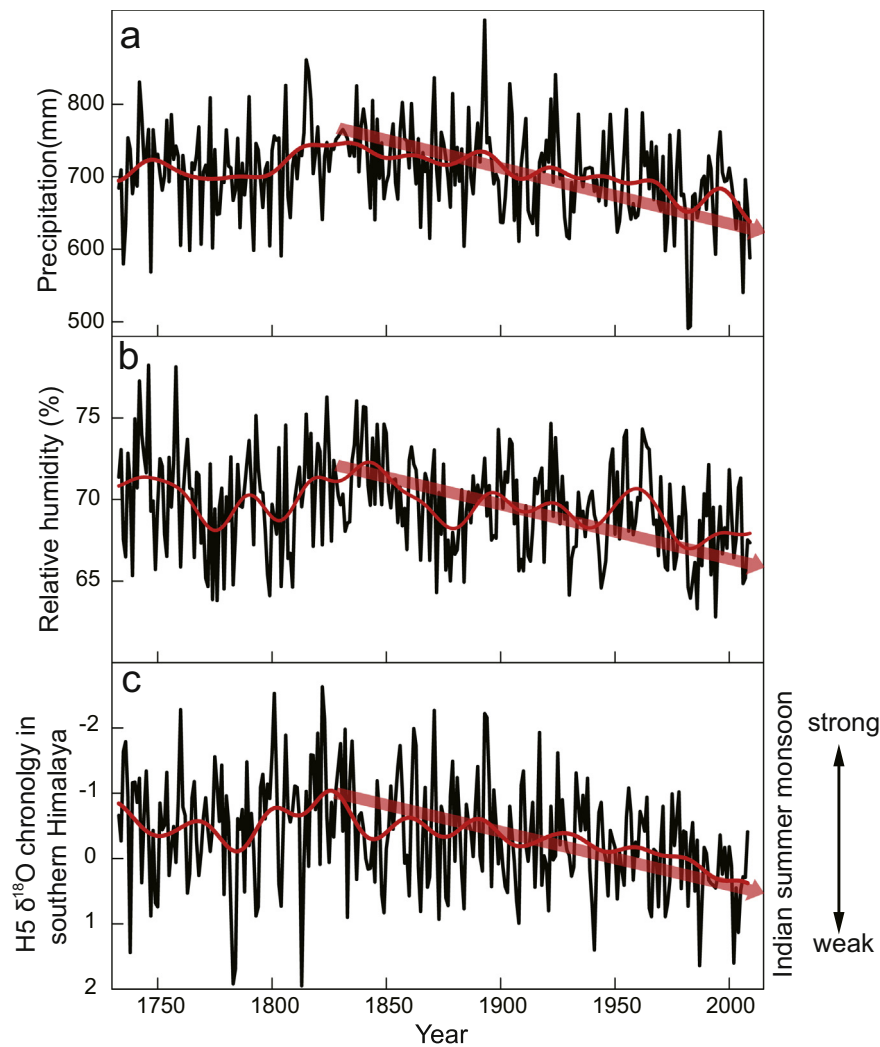


Fig. 5. Reconstructed regional rainy season precipitation in this study (a), and summer relative humidity reconstruction based on $\delta^{18}\text{O}_c$ in Batang (b, An et al., 2013), and H5 regional $\delta^{18}\text{O}_c$ in southern Himalaya (c, Xu et al., 2018a), and 11-year Fast Fourier Transform (FFT) smooth curves (red lines) emphasize decadal variations.

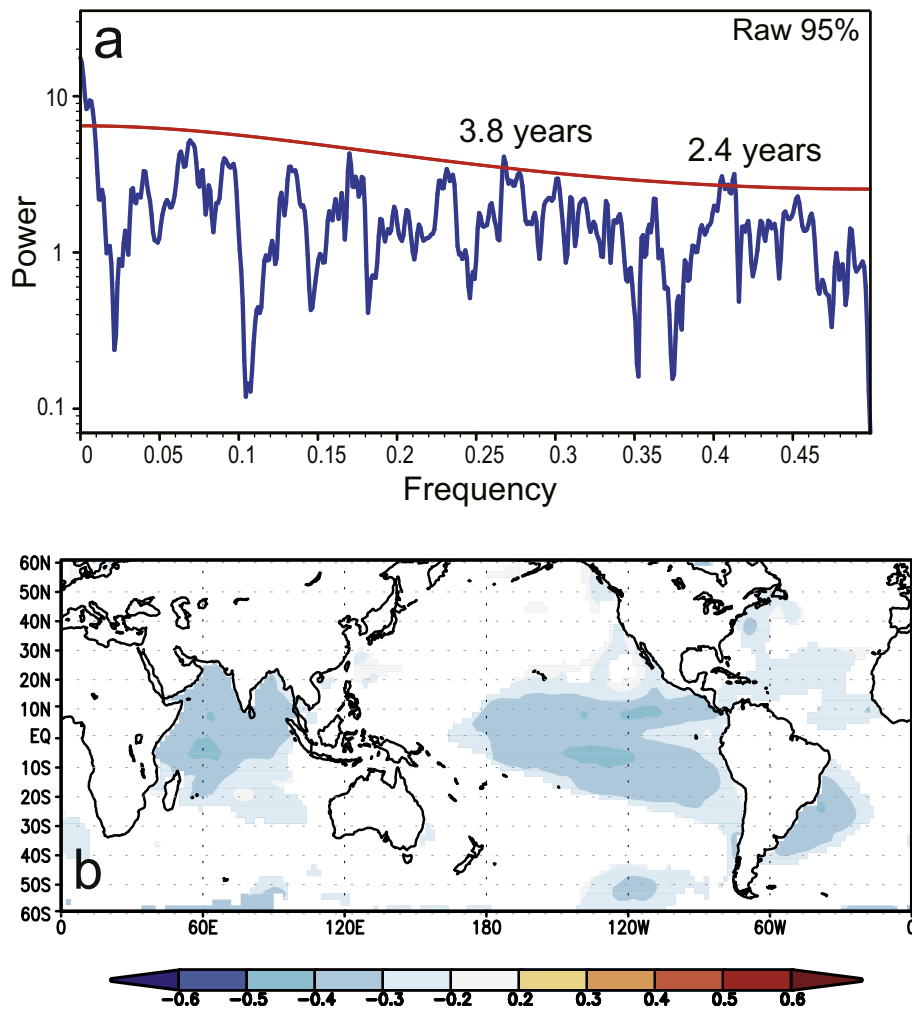


Fig. 6. Multi-taper power spectra for the reconstructed precipitation (a), spatial correlations between reconstructed precipitation and May–October sea surface temperature (SST, b).

Next, we averaged the six trees to produce the regional $\delta^{18}\text{O}_c$ chronology (LG $\delta^{18}\text{O}_c$ chronology) for the entire period and this is shown in Fig. 2d. Previous study in the southern Himalayas found no age-

related effects on $\delta^{18}\text{O}_c$ for Larch (Sano et al., 2013) and that detrending is not necessary for building up the $\delta^{18}\text{O}_c$ chronology there. The mean value and standard deviation of LG $\delta^{18}\text{O}_c$ chronology are 16.78‰ and

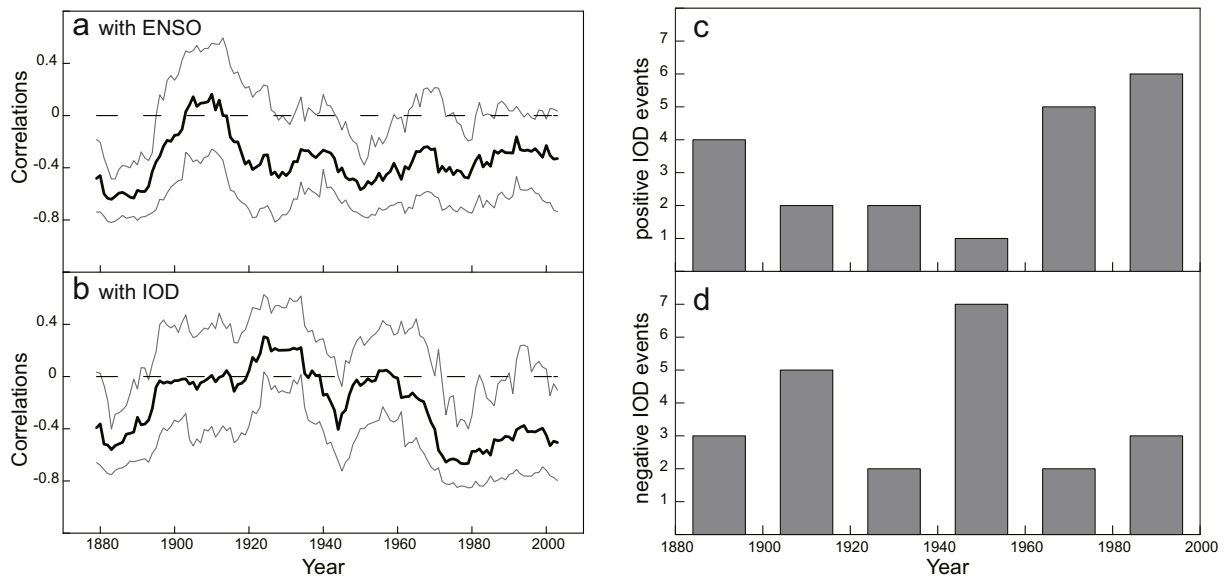


Fig. 7. 21-year running correlations between reconstructed precipitation and the El Niño–Southern Oscillation (ENSO, a), Indian Ocean dipole index (IOD, b), grey line indicates the 95% confidence level; positive (c) and negative (d) IOD events time series for every two decades (Hochreuther et al., 2016).

1.37‰. The first-order autocorrelation of LG $\delta^{18}\text{O}_c$ chronology is 0.23, which indicates that $\delta^{18}\text{O}_c$ in current year was not affected significantly by $\delta^{18}\text{O}_c$ in previous years. As verification of regional representativeness of LG $\delta^{18}\text{O}_c$ chronology, we also found that LG $\delta^{18}\text{O}_c$ chronology is positively correlated ($r = 0.55$, $p < 0.01$, 1733–2009) with the Batang spruce $\delta^{18}\text{O}_c$ chronology (located 330 km north of the study area, Fig. 1, by An et al., 2013). The mean $\delta^{18}\text{O}_c$ value between the two sites has a 4.6‰ difference, yet the standard deviation between the two $\delta^{18}\text{O}_c$ chronologies shows no significant difference. The main reason of the mean difference between two $\delta^{18}\text{O}_c$ chronologies lies in tree physiological differences, since $\delta^{18}\text{O}_c$ of larch was lower than $\delta^{18}\text{O}_c$ of spruce even in the same sampling site (Hochreuther et al., 2016; Li et al., 2011; Sano et al., 2013).

3.2. Climate implications of $\delta^{18}\text{O}_c$ and precipitation reconstruction

Correlations between LG $\delta^{18}\text{O}_c$ chronology and regional climatic parameters from previous October to current October during the period of 1959–2013 are shown in Fig. 3. During the rainy season (May–October), LG $\delta^{18}\text{O}_c$ chronology shows negative correlations with regional precipitation ($r = -0.68$, $p < 0.01$) and relative humidity ($r = -0.67$, $p < 0.01$), with positive correlations in VPD ($r = 0.58$, $p < 0.01$) and temperature ($r = 0.39$, $p < 0.01$). It should be noted that regional temperature has a close relationship with relative humidity ($r = -0.62$, $p < 0.01$, 1959–2013), VPD ($r = 0.61$, $p < 0.01$, 1959–2013) and precipitation ($r = -0.33$, $p < 0.05$, 1959–2013). Considering the strong $\delta^{18}\text{O}_c$ -relative humidity correlation and relatively weak $\delta^{18}\text{O}_c$ -temperature correlation, this temperature signal could be altered by the leaf water enrichment when the leaf responses to VPD, and the $\delta^{18}\text{O}_c$ -temperature correlation may be a byproduct of the close relationship between temperature and relative humidity and VPD.

Spatial correlation between rainy season precipitation (CRU and GPCC) and $\delta^{18}\text{O}_c$ was subsequently constructed and this is shown in Fig. S2. The results of different precipitation datasets indicate that LG $\delta^{18}\text{O}_c$ chronology does reflect the rainy season hydroclimate variation in a region encompassing the Southeast Tibet Plateau. Based on the mechanistic model of isotope fractionation in woody plants established by Roden et al. (2000), relative humidity and precipitation $\delta^{18}\text{O}$ does affect $\delta^{18}\text{O}_c$. Precipitation influences $\delta^{18}\text{O}_c$ through relative humidity and precipitation $\delta^{18}\text{O}$. Indeed, in this region the rainy season precipitation has a strong positive correlation with relative humidity ($r = 0.66$, $p < 0.01$, 1959–2013). Lower relative humidity enhances evapotranspiration and subsequently enriches leaf water ^{18}O that was recorded in cellulose $\delta^{18}\text{O}$ (An et al., 2013; Wernicke et al., 2015; Xu et al., 2018a, 2017). On the other hand, regional precipitation affected precipitation $\delta^{18}\text{O}$ by rainout processes, and when precipitation $\delta^{18}\text{O}$ signal transfer directly into the plant cellulose $\delta^{18}\text{O}_c$ during the processes of cellulose synthesis, and thus regional precipitation signal was preserved in $\delta^{18}\text{O}_c$ (Roden et al., 2000; Vuille et al., 2005). In short, higher rainfall associated with depleted precipitation $\delta^{18}\text{O}$ leads to lower $\delta^{18}\text{O}_c$, and this further lowers $\delta^{18}\text{O}_c$ by weakening evapotranspiration. Such negative correlations between $\delta^{18}\text{O}_c$ and regional rainy season precipitation have also been found in the Tibetan Plateau and throughout monsoon Asia (Sano et al., 2013, 2017; C. Xu et al., 2015; Xu et al., 2018b).

Since the rainy season precipitation has the highest correlations with $\delta^{18}\text{O}_c$, a simple linear regression model was used to estimate the transfer function between precipitation and $\delta^{18}\text{O}_c$ chronology:

$$P = -44.36 * O + 1450.9; (R^2 = 0.46, n = 54, p < 0.001)$$

where P represents regional May–October precipitation, and O is $\delta^{18}\text{O}_c$ chronology. The linear regression model explains 46% of the observed variance in May–October precipitation from four meteorological stations. Split calibration-verification test shows that r and R^2 are

significant, and RE and CE are positive for both sub-periods, which suggest that the regression model is valid (Table 1).

Based on the aforementioned regression model, we reconstructed the rainy season precipitation for the period 1733–2013. The mean value and standard deviation (σ) of the reconstructed series are 706.53 and 60.54 mm, respectively. The reconstructed precipitation shows good coherence with the observed precipitation (Fig. 4a), albeit short of capturing the extreme years of increased and decreased rainfall; this shortfall may be due to the inherent bias of regression model in the mean (Sun et al., 2017), reducing variance and underestimate extremes (Mccarroll et al., 2015).

An interdecadal variation is present in both records, showing that the rainy season precipitation decreased in 1959, increased in 1980, and then decreased again since 2000. The 31-year running correlation between reconstructed and observed precipitation appears to be significant and stable (Fig. 4b). For the full record since 1733, the reconstructed precipitation (Fig. 4c) was superimposed with an 11-year low-pass filter to highlight the decadal-scale fluctuations. Wet periods with precipitation above the mean value occurred in 1740–1760 and 1800–1900, while dry periods occurred in 1760–1800, 1950–2013. There is an apparent drying trend since around 1840, accompanied by a frequency increase of droughts after 1970. A deviation of 1σ from the mean was used as a threshold for determining extreme dry and wet events (Bao et al., 2012; Mokrria et al., 2017). Based on this criterion, there are 43 extreme dry and 36 wet events in the reconstruction. Here, we only list the top ten extreme dry and wet events in Table S3, and found 7 out of 10 extreme dry events happening since 1970. In contrast, all the extreme wet events occurred before 1924. These results have a profound implication that the hydroclimate of southwest China LLH may have entered a dry regime, at least compared to the past 280 years.

3.3. Comparison with other proxy records

To put the southwest China LLH record into regional perspective, we compared the reconstructed precipitation with previously published high-resolution summer relative humidity reconstruction in Batang, Sichuan province (An et al., 2013), and regional H5 $\delta^{18}\text{O}_c$ chronology composting of five $\delta^{18}\text{O}_c$ records in southern Himalaya (Xu et al., 2018a), the locations of which are shown in Fig. 1. The time series of these different data are shown in Fig. 5, including the rainy season precipitation reconstructed from LG $\delta^{18}\text{O}_c$ chronology (hereafter LG precipitation). The LG precipitation and summer relative humidity reconstruction in Batang are significantly correlated ($r = 0.55$, $p < 0.01$) during their common period of 1733–2009. Both the LG precipitation and the Batang relative humidity reconstruction show a decreasing trend since 1840. This result echoes previous findings (Chu et al., 2011; Wernicke et al., 2015) that the $\delta^{18}\text{O}_c$ record and the maar lake sediment record in Sichuan province also show decreased summer precipitation and relative humidity since around 1850.

Since the rainy season moisture in southwest China LLH is mainly transported from Bay of Bengal, the decreasing LLH rainfall may reflect fluctuations in the Indian summer monsoon. Thus, we further compared with the H5 $\delta^{18}\text{O}_c$ chronology including five $\delta^{18}\text{O}_c$ records collected in southern Himalaya as a proxy of the Indian summer monsoon, adopted from Xu et al. (2018a). As shown in Fig. 5c, H5 $\delta^{18}\text{O}_c$ chronology also indicates a weakening of the Indian summer monsoon since 1820. Given that the LG precipitation reconstruction is moderately correlated with the H5 $\delta^{18}\text{O}_c$ chronology ($r = -0.28$, $p < 0.01$) during their common period of 1733–2008, the results presented thus far suggest that the weakened Indian summer monsoon and the long-term drying in LLH are related.

3.4. Tropical ocean SST teleconnections with rainy season precipitation in southwest China

Spectral analysis of the LG precipitation, based on the multi-taper method (Mann and Lees, 1996) and shown in Fig. 6a, reveals

pronounced high frequencies at 3.8 and 2.4 years, as well as a very low frequency of >100 years; these are significant at a confidence level >95%. Those high frequency periodicities coincide with the interannual signals of ENSO and IOD. For instance, early-summer precipitation in LLH tends to decrease during El Niño (Liu et al., 2011; Yang et al., 2011) while whole-summer precipitation was observed to be reduced in LLH by positive IOD events (Cao et al., 2014; Qiu et al., 2014). Spatial correlations map computed between the LG precipitation reconstruction and SST during the rainy season (Fig. 6b) does show that positive SST anomaly (warming) in the central-eastern tropical Pacific and much of the Indian Ocean coexist with reduced LG precipitation. The decrease in regional precipitation associated with the warm phases of ENSO could be ascribed as an anomalous regional Hadley circulation, which features descending motion over the Indian continent and ascending motion near the equator, sustained by the anomalous Walker circulation in the equatorial Indian Ocean (Krishnamurthy and Goswami, 1999). In addition, warming in the Indian Ocean and Pacific could contribute to the weakening land–ocean gradient and thereby reduce the amount of precipitation over parts of South Asia (Xu et al., 2018a, 2018b). However, the ENSO–Indian summer monsoon relationship has changed since 1970s from the more important role of east Pacific El Niño to the recent increase in the influence of central Pacific El Niño (Kumar et al., 2006).

Given that the relationship between Indian summer monsoon and ENSO and IOD has changed (Ashok et al., 2001; Kumar et al., 1999), we further computed the 21-year sliding correlations between the LG precipitation and ENSO/IOD index during the period of 1870–2013, which are shown in Fig. 7a/b. Here the ENSO index was determined by the Niño-3.4 SST anomaly. The LG precipitation showed significant correlations with ENSO in the period of 1870–1895 and 1915–2013 except for the period of 1895–1915. The LG precipitation–IOD relationship was weak during the period of 1880–1970 and became strong since 1970.

Different phases of IOD have asymmetrical impacts on rainfall in southern China, as positive IOD phase influences more strongly than negative IOD phase does (Qiu et al., 2014). The frequency of positive IOD events that reduced rainfall in southwest China has increased since 1960 (Hochreuther et al., 2016; Qiu et al., 2014), as shown in Fig. 7c, and this may contribute to the apparent increase in drought events due to the significant IOD–rainfall relationship (recall Fig. 4c and Table S3). Previous $\delta^{18}\text{O}_c$ record in the southeastern Tibetan Plateau also showed positive correlations with IOD during periods of strong positive IOD (Hochreuther et al., 2016). Given that climate model simulations suggested that the frequency of extreme positive IOD event will increase under global warming (Cai et al., 2014, 2018), the persistent positive correlation between IOD and LHH drought identified here implies potentially more or enhanced drought in southwest China LLH in the face of future warming.

4. Conclusion

Six highly intercorrelated $\delta^{18}\text{O}_c$ time series from Larix were used to develop the LG $\delta^{18}\text{O}_c$ chronology for the period 1733–2013 in Yunnan, southwest China. The LG $\delta^{18}\text{O}_c$ chronology showed negative correlations with regional May–October precipitation, relative humidity, scPDSI and SPEI during the period of 1959–2013, with stable sliding correlations of the May–October precipitation. The LG $\delta^{18}\text{O}_c$ chronology accounts for 46% of the observed variance in precipitation during 1959–2013, and the linear reconstruction model passed strict calibration–verification test. Based on this model, rainy season precipitation was reconstructed back to 1733. The precipitation reconstruction revealed a discernable drying trend since 1840, which is consistent with other $\delta^{18}\text{O}_c$ records. This result also echoes the documented reduction in the Indian summer monsoon during the recent decades observed from independent data sources.

Spatial correlation and sliding correlation analyses showed that rainy-season precipitation reconstruction was modulated collectively

by ENSO and IOD at inter-annual time scale, with differing degree of influence decade-by-decade. The observed enhancement in the drought–IOD relationship since 1970 may be related to the increase in positive IOD events since 1970. The increased frequency of positive IOD events, when coupled with the global warming trend, implies that southwest China LLH may see an increase in, or more severe droughts in the future. Further research based on coupled-model experiments is needed to validate this implication.

Acknowledgement

We deeply appreciate the helpful comments from two anonymous reviewers and editor to improve the manuscript. The project was supported by Natural Science Foundation of China (Grant No. 41672179, 41672352, 41630529, 41430531, 41690114, 41888101), the Strategic Priority Research Program of Chinese Academy of Sciences (Grant No. XDB26020000, XDA13010106), the Chinese Academy of Sciences (CAS) Pioneer Hundred Talents Program, the National Key R&D Program of China (Grant No. 2016YFA0600502, 2017YFE0112800). No potential conflict of interest was reported by the authors.

Appendix A. Supplementary data

Supplementary data to this article can be found online at <https://doi.org/10.1016/j.scitotenv.2019.01.186>.

References

- An, W., Liu, X., Leavitt, S., Ren, J., Sun, W., Wang, W., Wang, Y., Xu, G., Chen, T., Qin, D., 2012. Specific climatic signals recorded in earlywood and latewood $\delta^{18}\text{O}$ of tree rings in southwestern China. *Tellus Ser. B Chem. Phys. Meteorol.* 64 (1), 18703. <https://doi.org/10.3402/tellusb.v64i0.18703>.
- An, W., Liu, X., Leavitt, S.W., Xu, G., Zeng, X., Wang, W., Qin, D., Ren, J., 2013. Relative humidity history on the Batang–Litang Plateau of western China since 1755 reconstructed from tree-ring $\delta^{18}\text{O}$ and δD . *Clim. Dyn.* 42 (9–10), 2639–2654.
- Araguas-Araguas, L., Froehlich, K., Rozanski, K., 1998. Stable isotope composition of precipitation over Southeast Asia. *J. Geophys. Res.* 103 (D22), 28721.
- Ashok, K., Guan, Z., Yamagata, T., 2001. Impact of the Indian Ocean dipole on the relationship between the Indian monsoon rainfall and ENSO. *Geophys. Res. Lett.* 28 (23), 4499–4502.
- Bao, G., Liu, Y., Liu, N., 2012. A tree-ring-based reconstruction of the Yimin River annual runoff in the Hulun Buir region, Inner Mongolia, for the past 135 years. *Chin. Sci. Bull.* 57, 4765–4775.
- Cai, W., Santoso, A., Wang, G., Weller, E., Wu, L., Ashok, K., Masumoto, Y., Yamagata, T., 2014. Increased frequency of extreme Indian Ocean Dipole events due to greenhouse warming. *Nature* 510 (7504), 254–258.
- Cai, W., Wang, G., Gan, B., Wu, L., Santoso, A., Lin, X., Chen, Z., Jia, F., Yamagata, T., 2018. Stabilised frequency of extreme positive Indian Ocean Dipole under 1.5 °C warming. *Nat. Commun.* 9 (1), 1419.
- Cao, J., Yao, P., Wang, L., Liu, K., 2014. Summer rainfall variability in low-latitude highlands of China and subtropical Indian Ocean Dipole. *J. Clim.* 27 (2), 880–892.
- Chu, G., Sun, Q., Yang, K., Li, A., Yu, X., Xu, T., Yan, F., Wang, H., Liu, M., Wang, X., 2011. Evidence for decreasing South Asian summer monsoon in the past 160 years from varved sediment in Lake Xinluhai, Tibetan Plateau. *J. Geophys. Res.* 116 (D2), D02116.
- Cook, E.R., Meko, D.M., Stahle, D.W., Cleaveland, M.K., 1999. Drought reconstructions for the continental United States. *J. Clim.* 12 (4), 1145–1162.
- Fan, Z.X., Achim, B., Cao, K.F., 2010. Tree-ring based drought reconstruction in the central Hengduan Mountains Region (China) since A.D. 1655. *Int. J. Climatol.* 28 (14), 1879–1887.
- Fang, K., Gou, X., Chen, F., Li, J., D'Arrigo, R., Cook, E., Yang, T., Davi, N., 2010. Reconstructed droughts for the southeastern Tibetan Plateau over the past 568 years and its linkages to the Pacific and Atlantic Ocean climate variability. *Clim. Dyn.* 35 (4), 577–585.
- Gou, X.H., Tao, Y., Gao, L.L., Yang, D., Yang, M.X., Chen, F.H., 2013. A 457-year reconstruction of precipitation in the southeastern Qinghai–Tibet Plateau, China using tree-ring records. *Sci. Bull.* 58 (10), 1107–1114.
- Harris, I., Jones, P., Osborn, T., Lister, D., 2014. Updated high-resolution grids of monthly climatic observations—the CRU TS3. 10 Dataset. *Int. J. Climatol.* 34 (3), 623–642.
- Hochreuther, P., Wernicke, J., Griesinger, J., Mölg, T., Zhu, H., Wang, L., Bräuning, A., 2016. Influence of the Indian Ocean Dipole on tree-ring $\delta^{18}\text{O}$ of monsoonal Southeast Tibet. *Clim. Chang.* 137 (1–2), 217–230.
- Hogg, E.H., 1997. Temporal scaling of moisture and the forest–grassland boundary in western Canada. *Agric. For. Meteorol.* 84, 115–122.
- Hogg, E.H., Barr, G., Black, T.A., 2013. A simple soil moisture index for representing multi-year drought impacts on aspen productivity in the western Canadian interior. *Agric. For. Meteorol.* 178, 173–182.
- Holmes, R., 1983. Computer-assisted quality control in tree-ring dating and measurement. *Tree-Ring Bull.* 43 (1), 69–78.

- Krishnamurthy, V., Goswami, B.N., 1999. Indian monsoon-ENSO relationship on interdecadal timescale. *J. Clim.* 13, 579–595.
- Kumar, K.K., Rajagopalan, B., Cane, M.A., 1999. On the weakening relationship between the Indian monsoon and ENSO. *Science* 284 (5423), 2156–2159.
- Kumar, K.K., Rajagopalan, B., Hoerling, M., Bates, G., Cane, M., 2006. Unraveling the mystery of Indian monsoon failure during El Niño. *Science* 314 (5796), 115–119.
- Leavitt, S., 2010. Tree-ring C-H-O isotope variability and sampling. *Sci. Total Environ.* 408, 5244–5253.
- Li, Q., Nakatsuka, T., Kawamura, K., Liu, Y., Song, H., 2011. Regional hydroclimate and precipitation $\delta^{18}\text{O}$ revealed in tree-ring cellulose $\delta^{18}\text{O}$ from different tree species in semi-arid northern China. *Chem. Geol.* 282 (1–2), 19–28.
- Li, J., Shi, J., Zhang, D.D., Yang, B., Fang, K., Yue, P.H., 2017. Moisture increase in response to high-altitude warming evidenced by tree-rings on the southeastern Tibetan Plateau. *Clim. Dyn.* 48 (1–2), 649–660.
- Liu, L., Yang, R.W., Xing, D., Cao, J., 2011. The influence of developing and decaying stage of ENSO and summer precipitation in Yunnan (in Chinese). *J. Trop. Meteorol.* 27 (2), 278–282.
- Liu, X., Zeng, X., Leavitt, S.W., Wang, W., An, W., Xu, G., 2013. A 400-year tree-ring $\delta^{18}\text{O}$ chronology for the southeastern tibetan plateau: implications for inferring variations of the regional hydroclimate. *Glob. Planet. Chang.* 104, 23–33.
- Liu, J., Ren, H.-L., Li, W., Zuo, J., 2018. Remarkable impacts of Indian Ocean Sea surface temperature on interdecadal variability of summer rainfall in southwestern China. *Atmosphere* 9 (3), 103.
- Mann, M.E., Lees, J.M., 1996. Robust estimation of background noise and signal detection in climatic time series. *Clim. Chang.* 33 (3), 409–445.
- Mccarroll, D., Young, G.H.F., Loader, N.J., 2015. Measuring the skill of variance-scaled climate reconstructions and a test for the capture of extremes. *The Holocene* 25 (4), 618–626.
- Mokria, M., Gebrekirstos, A., Abiyu, A., Noordwijk, M.V., Bräuning, A., 2017. Multi-century tree-ring precipitation record reveals increasing frequency of extreme dry events in the upper Blue Nile River catchment. *Glob. Chang. Biol.* 23 (12), 5436–5454.
- Peng, J., Zhang, Q., Bueh, C., 2007. On the characteristics and possible causes of a severe drought and heat wave in the Sichuan-Chongqing region in 2006. *Climatic Environ. Res.* 12 (3), 464–474.
- Qiu, Y., Cai, W., Guo, X., Ng, B., 2014. The asymmetric influence of the positive and negative IOD events on China's rainfall. *Sci. Rep.* 4 (4), 4943.
- Roden, J.S., Lin, G., Ehleringer, J.R., 2000. A mechanistic model for interpretation of hydrogen and oxygen isotope ratios in tree-ring cellulose. *Geochim. Cosmochim. Acta* 64 (1), 21–35.
- Saji, N.H., Goswami, B.N., Vinayachandran, P.N., Yamagata, T., 1999. A dipole mode in the tropical Indian Ocean. *Nature* 401 (6751), 360–363.
- Sano, M., Tshering, P., Komori, J., Fujita, K., Xu, C., Nakatsuka, T., 2013. May–September precipitation in the Bhutan Himalaya since 1743 as reconstructed from tree ring cellulose $\delta^{18}\text{O}$. *J. Geophys. Res. Atmos.* 118 (15), 8399–8410.
- Sano, M., Dimri, A.P., Ramesh, R., Xu, C., Li, Z., Nakatsuka, T., 2017. Moisture source signals preserved in a 242-year tree-ring $\delta^{18}\text{O}$ chronology in the western Himalaya. *Glob. Planet. Chang.* 157, 73–82.
- Schneider, U., Becker, A., Finger, P., Meyer-Christoffer, A., Rudolf, B., Ziese, M., 2015. GPCC Full Data Reanalysis Version 7.0 at 0.5°: Monthly Land-surface Precipitation From Rain-gauges Built on GTS Based and Historic Data. https://doi.org/10.5676/DWD_GPCC/FD_M_V7_050.
- Sheng, E., Yu, K., Xu, H., Lan, J., Liu, B., Che, S., 2015. Late Holocene Indian summer monsoon precipitation history at Lake Lugu, northwestern Yunnan Province, southwestern China. *Palaeogeogr. Palaeoclimatol. Palaeoecol.* 438, 24–33.
- Shi, C., Daux, V., Zhang, Q., Risi, C., Hou, S., Stievenard, M., Pierre, M., Li, Z., Masson-Delmotte, V., 2012. Reconstruction of southeast Tibetan Plateau summer climate using tree ring $\delta^{18}\text{O}$: moisture variability over the past two centuries. *Clim. Past.* 8, 205–213.
- Smith, T., Reynolds, R., Peterson, T., Lawrimore, J., 2008. Improvements to NOAA's historical merged land-ocean surface temperature analysis. *J. Clim.* 21 (10), 2283–2296.
- Sun, C., Yang, S., 2012. Persistent severe drought in southern China during winter-spring 2011: large-scale circulation patterns and possible impacting factors. *J. Geophys. Res. Atmos.* 117, D10112. <https://doi.org/10.1029/2012JD017500>.
- Sun, Y., Bekker, M., DeRose, J.R., Kjelgren, R., Wang, S.-Y., 2017. Statistical treatment for the wet bias in tree-ring chronologies - a case study from the Interior West, USA. *Environ. Ecol. Stat.* 24, 131–150.
- Vuille, M., Werner, M., Bradley, R., Keimig, F., 2005. Stable isotopes in precipitation in the Asian monsoon region. *J. Geophys. Res.* 110 (D23), D23108.
- Wang, Z., Yang, B., Deslauriers, A., Qin, C., He, M., Shi, Liu, J., 2012. Two phases of seasonal stem radius variations of *Sabina przewalskii* Kom. in northwestern China inferred from sub-diurnal shrinkage and expansion patterns. *Trees* 26, 1747–1757.
- Wang, L., Chen, W., Zhou, W., Huang, G., 2016. Understanding and detecting super-extreme droughts in Southwest China through an integrated approach and index. *Q. J. R. Meteorol. Soc.* 142 (694), 529–535.
- Wernicke, J., Grießinger, J., Hochreuther, P., Bräuning, A., 2015. Variability of summer humidity during the past 800 years on the eastern Tibetan Plateau inferred from $\delta^{18}\text{O}$ of tree-ring cellulose. *Clim. Past* 10 (4), 327–356.
- Wigley, T., Briffa, K., Jones, P., 1984. On the average value of correlated time series, with applications in dendroclimatology and hydrometeorology. *J. Clim. Appl. Meteorol.* 23 (2), 201–213.
- Xu, C., Sano, M., Nakatsuka, T., 2011. Tree ring cellulose $\delta^{18}\text{O}$ of *Fokienia hodginsii* in northern Laos: a promising proxy to reconstruct ENSO? *J. Geophys. Res.* 116 (D24), D24109.
- Xu, H., Hong, Y., Hong, B., 2012. Decreasing Asian summer monsoon intensity after 1860 AD in the global warming epoch. *Clim. Dyn.* 39 (7–8), 2079–2088.
- Xu, C., Zheng, H., Nakatsuka, T., Sano, M., 2013. Oxygen isotope signatures preserved in tree ring cellulose as a proxy for April–September precipitation in Fujian, the subtropical region of Southeast China. *J. Geophys. Res. Atmos.* 118 (23), 12,805–812,815.
- Xu, C., Pumijumnong, N., Nakatsuka, T., Sano, M., Li, Z., 2015. A tree-ring cellulose $\delta^{18}\text{O}$ -based July–October precipitation reconstruction since AD 1828, Northwest Thailand. *J. Hydrol.* 529, 433–441.
- Xu, H., Zhou, X., Lan, J., Liu, B., Sheng, E., Yu, K., Peng, C., Feng, W., Hong, B., Yeager, K.M., 2015. Late Holocene Indian summer monsoon variations recorded at Lake Erhai, southwestern China. *Quat. Res.* 83 (2), 307–314.
- Xu, C., Ge, J., Nakatsuka, T., Yi, L., Zheng, H., Sano, M., 2016. Potential utility of tree ring $\delta^{18}\text{O}$ series for reconstructing precipitation records from the lower reaches of the Yangtze River, Southeast China. *J. Geophys. Res. Atmos.* 121 (8), 3954–3968.
- Xu, C., Zhu, H., Nakatsuka, T., Sano, M., Li, Z., Shi, F., Liang, E., Guo, Z., 2017. Sampling strategy and climatic implication of tree-ring cellulose oxygen isotopes of *Hippophae tibetana* and *Abies georgei* on the southeastern Tibetan Plateau. *Int. J. Biometeorol.* (s1–4), 1–8.
- Xu, C., Sano, M., Dimri, A.P., Ramesh, R., Nakatsuka, T., Shi, F., Guo, Z., 2018a. Decreasing Indian summer monsoon on the northern Indian sub-continent during the last 180 years: evidence from five tree-ring cellulose oxygen isotope chronologies. *Clim. Past* 14 (5), 653–664.
- Xu, C., Shi, J., Zhao, Y., Nakatsuka, T., Sano, M., Shi, S., Guo, Z., 2018b. Early summer precipitation in the lower Yangtze River basin for AD 1845–2011 based on tree-ring cellulose oxygen isotopes. *Clim. Dyn.* 1–12.
- Yang, Y., Man, Z., Zheng, J., 2007. Reconstruction of the starting time series of rainy season in Yunnan and the evolution of summer monsoon during 1711–1982. *J. Geogr. Sci.* 17 (2), 212–220.
- Yang, Y., Yan, D.U., Chen, H., 2011. Influence of ENSO event on rainfall anomaly over Yunnan Province and its neighboring regions during late spring-early summer. *Chin. J. Atmos. Sci.* 35 (4), 729–738.
- Yang, J., Gong, D., Wang, W., Hu, M., Mao, R., 2012. Extreme drought event of 2009/2010 over southwestern China. *Meteorol. Atmos. Phys.* 115 (3–4), 173–184.